DOI: 10.6060/tcct.2017601.5518

Для цитирования:
Ефремов А.М., Квон К.-Х. Параметры и состав плазмы в смеси $CF_4/O_2/Ar$. *Изв. вузов. Химия и хим. технология.* 2017. Т. 60. Вып. 1. С. 50–55.

For citation:
Efremov A.M., Kwon K.-H. Plasma parameters and composition in $CF_4/O_2/Ar$ gas mixture. *Izv. Vyssh. Uchebn. Zaved. Khim. Khim. Tekhnol*. 2017. V. 60. N 1. P. 50–55.

УДК: 537.525

А.М. Ефремов, К.-Х. Квон

Александр Михайлович Ефремов (✉)

Кафедра технологии приборов и материалов электронной техники, Ивановский государственный химико-технологический университет, Шереметевский просп., 7, Иваново, Российская Федерация, 153000
E-mail: efremov@isuct.ru (✉)

Kwang-Ho Kwon

Department of Control and Instrumentation Engineering, Korea University, Sejong 339-700, South Korea.
E-mail: kwonkh@korea.ac.kr

ПАРАМЕТРЫ И СОСТАВ ПЛАЗМЫ В СМЕСИ $CF_4/O_2/Ar$

Изучено влияние соотношения концентраций O_2/Ar в смеси $CF_4/O_2/Ar$ на параметры плазмы и потоки активных частиц, определяющие кинетику сухого травления в данной системе. Исследования проводились с использованием совокупности методов диагностики и моделирования плазмы. Было найдено, что замещение аргона на кислород при постоянном содержании CF_4 в плазмообразующей смеси не приводит к немонотонным изменениям концентрации атомов F, как это неоднократно сообщалось для бинарных смесей CF_4/O_2. Подробно рассмотрен механизм данного явления и его возможное влияние на кинетику травления и плазменной полимеризации.

Ключевые слова: CF_4, плазма, диагностика, моделирование, кинетика реакций

UDC: 537.525

A.M. Efremov, K.-H. Kwon

Alexandr M. Efremov (✉)

Department of Electronic Devices and Materials Technology, Ivanovo State University of Chemistry and Technology, Sheremetevsky ave., 7, Ivanovo, 153000, Russia
E-mail: efremov@isuct.ru (✉)

Kwang-Ho Kwon

Dept. of Control and Instrumentation Engineering, Korea University, Sejong 339-700, South Korea.
E-mail: kwonkh@korea.ac.kr

PLASMA PARAMETERS AND COMPOSITION IN $CF_4/O_2/Ar$ GAS MIXTURE

The effects of O_2/Ar mixing ratio in $CF_4/O_2/Ar$ mixture on both plasma parameters and fluxes of active species determining the dry etching kinetics in this gas system were analyzed. The investigation combined plasma diagnostics by Langmuir probes and zero-dimensional plasma modeling. It was found that the substitution of Ar with O_2 at constant fraction of CF_4 in a feed gas does not result in the non-monotonic change in F atom density, as it was repeatedly reported for the binary CF_4/O_2 gas mixtures. The mechanisms of this phenomenon as well as its possible impact on the etching/polymerization kinetics were discussed in details.

Key words: CF_4 plasma, diagnostics, modeling, reaction kinetics

INTRODUCTION

Fluorocarbon (FC) gases, such as CF_4 and other ones, are widely used in the microelectronic industry for dry patterning of silicon wafers and dielectric (SiO_2, Si_3N_4) thin films [1, 2]. From Refs. [2-4], it can be understood that the FC gases are frequently combined with O_2 with the aim of increasing the F atoms yield and suppressing polymerization on the surfaces which are in a contact with plasma. Really, there are many experimental evidences that the addition of O_2 to the CF_4-based gas mixture results in the non-monotonic behavior of the F atom density which exhibits a maximum at 20-40% O_2 [5-9]. Most authors reasonably attribute this effect to the stepwise dissociation of the CF_x species due to their interaction with oxygen atoms [6, 9].

Recently, in order to satisfy the increasingly demanding requirements concerning device dimensions and performance, many dry etching processes require optimization through the appropriate choice of working gas and input process conditions. In this framework, an understanding of the plasma chemistry mechanisms involved in various gas systems is important for future progress. When analyzing the published works, one can conclude that the effect of O_2 on the plasma parameters and composition has been well studied only for binary (CF_4/O_2) or ternary ($CF_4/O_2/Ar$) gas mixtures where an increase in the O_2 mixing ratio is accompanied by a proportionally decreasing CF_4 gas fraction. At the same time, the ternary gas systems provide more pathways for the changes in gas mixing ratios in order to obtain the optimal process conditions. For example, one can keep the fraction of CF_4 gas constant, but change the ratio between O_2 and Ar. It is clear that, since the composition of the feed gas is different compared with the simple CF_4/O_2 mixture, some principal differences in plasma parameters (through the electron energy distribution function and mean electron energy) and densities of plasma active species can take place. This is why the relationships between the plasma parameters and the composition for of the three-component $CF_4/O_2/Ar$ gas mixture with an CF_4 gas component of constant magnitude require additional investigation.

In this work, we performed the model-based study of $CF_4/O_2/Ar$ inductively coupled plasma aimed at understanding how the substitution of Ar for O_2 at fixed 50% content of CF_4 influences plasma parameters and densities of active species. The main attention was focused on the parameters directly influencing dry etching mechanisms: ion energy flux, F atom flux, polymerizing species (CF_2 and CF) flux as well as various flux-to-flux ratios illustrating the changes in the etching/polymerization balance. We also attempted the analysis of the formation-decay kinetics for neutral species in order to explain the obtained phenomena.

EXPERIMENTAL AND MODELING DETAILS

Experimental setup and procedures

The experiments were performed in a planar inductively coupled plasma (ICP) reactor used in previous work [10, 11]. The reactor had a cylindrical chamber (r = 15 cm), made from anodized aluminum. A 5-turn-copper coil was located on the top of the chamber, above the 10-mm-thick horizontal quartz window. The coil was connected to a 13.56 MHz power supply in order to sustain the plasma. The distance, l, between the window and the bottom electrode, which was used as a substrate holder, was 12.8 cm. The bottom electrode was connected to another 12.56 MHz power supply in order to control the negative dc bias on the etched wafer.

The experiments were performed at a fixed total gas flow rate (q = 40 sccm), gas pressure (p = 6 mTorr), and input power (W = 900 W). The input power density $W' = W/\pi r^2 l$ then became 0.9 W/cm^3. In order to

imitate actual etching conditions, the bottom electrode was biased by W_{dc} = 200 W. The CF_4/O_2/Ar gas compositions were set by adjusting the partial flow rates. Particularly, the CF_4 flow rate was fixed at 20 sccm while the flow rates of the O_2 and Ar were variably set to a combined total of $q_{O2} + q_{Ar}$ = 20 sccm. Therefore, the proportion of CF_4 ($y_{CF4} = q_{CF4}/q$) in the feed gas was always 0.5, and the remaining half gas mixture was composed of various amounts of Ar and O_2

The plasma parameters were determined by a double Langmuir probe (LP), (DLP2000, Plasmart Inc.). The probe tip was installed through a hole in the sidewall of the chamber, 5.7 cm above the bottom electrode and centered in a radial direction. In order to ensure that the LP results were not affected by the formation of the FC polymer film on the tip surface, we conducted a set of preliminary experiments, where the current – voltage (I – V) curves were recorded continuously at fixed-feed gas composition and operating parameters. Even for the non-oxygenated plasmas, the differences between the results of such measurements did not exceed the standard experimental error for a period of at least 10 min after the plasma was turned on. Also, throughout the main experimental procedure, the probe tip was cleaned in 50% Ar + 50% O_2 plasma before and after each measurement. The output data were the electron temperature (T_e), ion current density (J_+), floating potential (U_f), and total positive ion density (n_+). The treatment of the I – V curves was based on Johnson & Malter's double probe theory [12], and the Allen-Boyd-Reynolds (ABR) approximation for the ion saturation current density [13]. These assume $J_+ \approx 0.61 e n_+ \upsilon$, where υ is the ion Bohm velocity. In our previous studies [10, 11], it was shown that such an approach can be reasonably applied even for more electronegative plasmas than those used in this study. The effective ion mass needed to determine υ was evaluated simply through the mole fractions of the corresponding neutral species.

Plasma modeling

To obtain the densities of the active species, we developed a simplified zero-dimensional model operating with the volume-averaged plasma parameters. Similarly, to our previous works [10, 11, 14, 15], the model was based on the Maxwellian electron energy distribution function (EEDF), and directly used the experimental data of T_e and n_+ as input parameters. Though the real EEDFs are not exactly Maxwellian, such a simplification for CF_4-based and low-pressure (p < 50 mTorr) ICPs provides reasonable agreement between the diagnostic results and modeling [10-12, 16, 27].

The general model assumptions as well as the reaction scheme were the same with our previous works [14, 15]. The rate coefficients for electron impact reactions were calculated as functions of Te using the fitting expressions in a form of $k = AT_e^B \exp(-C/T_e)$ [5, 14]. The heterogeneous chemistry of atoms (F, C, O) and radicals (CF_3, CF_2, CF) was described in terms of the conventional first-order recombination kinetics. The corresponding ticking probabilities were obtained from Refs [5, 14, 15]. The electron density (n_e) was calculated using the simultaneous solution of the steady-state chemical kinetic equation for negative ions $\nu_{da} n_e \approx k_{ii} n_+ n_-$ and the quasi-neutrality equation $n_+ = n_e + n_-$. These allow one to obtain

$$n_e \approx \frac{k_{ii} n_+^2}{\nu_{da} + k_{ii} n_+},$$

where $\nu_{da} \approx k_1 n_{CF4} + k_2 n_{O2}$ is the total frequency of dissociative attachment (R1: $CF_4 + e \rightarrow CF_3 + F^-$ and R2: $O_2 + e \rightarrow O + O^-$), n_- is the density of negative ions, and $k_{ii} \approx 1 \cdot 10^{-7}$ cm^3/s is the rate coefficient for ion-ion recombination. The steady-state densities for neutral ground-state plasma components were obtained from the system of chemical kinetics equations in the general form of $R_F - R_D = (k_s + 1/\tau_R)n$, where R_F and R_D are the volume-averaged formation and decay rates in bulk plasma for a given type of species, n is their density, k_s is the first-order heterogeneous decay rate coefficient, and $\tau_R = \pi r^2 lp/q$ is the residence time.

RESULTS AND DISCUSSION

Fig. 1 represents measured and model-predicted plasma parameters as functions of O_2 fraction in CF_4/O_2/Ar gas mixture. It can be seen that the substitution of Ar for O_2 results in decreasing both T_e (3.6-3.4 eV for 0-50% O_2, Fig. 1(a)) and J_+ (1.45-1.29 mA/cm^2 for 0-50% O_2, Fig. 1(a)) that corresponds to $n_+ = 5.7 \cdot 10^{10}$-$4.4 \cdot 10^{10}$ cm^{-3} (Fig. 1(b)). The model-predicted electron density follows the behavior n_+ and changes as $4.4 \cdot 10^{10}$-$2.8 \cdot 10^{10}$ cm^{-3} for 0-50% O_2. A decrease in electron temperature toward O_2-rich plasmas is probably results from an increase in the electron energy loss due to the low-threshold excitations (vibrational, electronic) for O_2 and other molecular species, which appear in a gas phase as products of plasma chemical reactions. The same behavior of both n_+ and n_e also looks quite reasonable and may be caused by a combination of at least two phenomena. First, the decreasing T_e suppresses ionization through decreasing the ionization rate coefficients for all types of neutral species. The high sensitivity of the ionization rate coefficients to T_e is because $\varepsilon_{iz} \approx$ 12-15 eV > $(3/2)T_e$ where ε_{iz} is the threshold energy for ionization

[5, 16], and (3/2)T_e is the mean electron energy. Secondly, the substitution of Ar for O_2 results in an increase in the densities of electronegative species (n_-/n_e = 0.28-0.58 for 0-50% O_2, Fig. 1(b)). This accelerates the decay rates of the positive ions and electrons through ion-ion recombination and dissociative attachment, respectively.

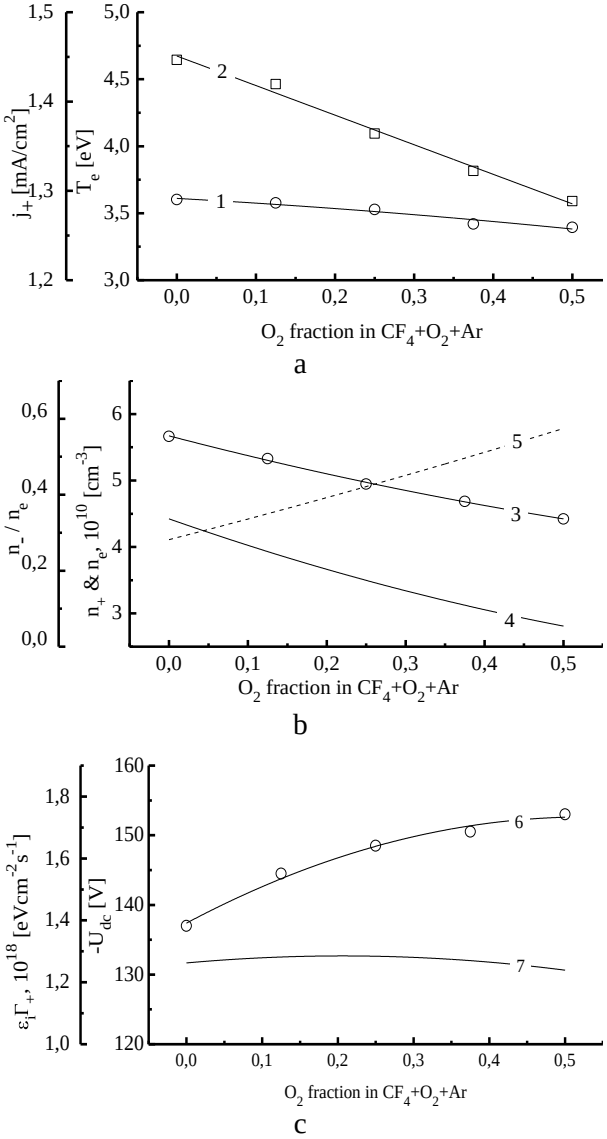

Fig. 1. Measured (lines + symbols) and model-predicted (lines) plasma parameters as function of O_2 fraction in CF_4 + O_2 + Ar gas mixture: 1–electron temperature, 2–ion current density, 3–total positive ion density, 4–electron density, 5–relative density of negative ions, 6–negative dc bias, 7–ion energy flux density

Рис. 1. Измеренные (линии + символы) и расчетные (линии) параметры плазмы как функции доли O_2 в плазмообразующей смеси CF_4 + O_2 + Ar: 1–температура электронов, 2–плотность ионного тока, 3–суммарная концентрация положительных ионов, 4–концентрация электронов, 5–относительная концентрация отрицательных ионов, 6–отрицательное смещение на подложкодержателе, 7–плотность потока энергии ионов

Fig. 2 illustrates the influence of O_2 content in the $CF_4/Ar/O_2$ gas mixture on the densities of neutral species. In the non-oxygenated 50% CF_4 + 50% Ar plasma, the main source of F atoms are the electron-impact dissociations of CF_4 (R3: $CF_4 + e \rightarrow CF_3 + F + e$, R4: $CF_4 + e \rightarrow CF_3^+ + F + 2e$) and CF_3 (R5: $CF_3 + e \rightarrow CF_2 + F + e$). These processes constitute approximately 86% of the total F atom formation rate while the contribution from the CF_2 and CF radicals through R6: $CF_2 + e \rightarrow CF + F + e$ and R7: $CF + e \rightarrow C + F + e$ does not exceed 5%. The remaining 9% comes from R8: $F_2 + e \rightarrow 2F + e$, which is supported by the high $F \rightarrow F_2$ recombination rate on the reactor walls. Accordingly, the decay of F atoms is mainly caused by their heterogeneous recombination while the rate of the fastest bulk process R9: $CF_3 + F \rightarrow CF_4$ is about 10 times less.

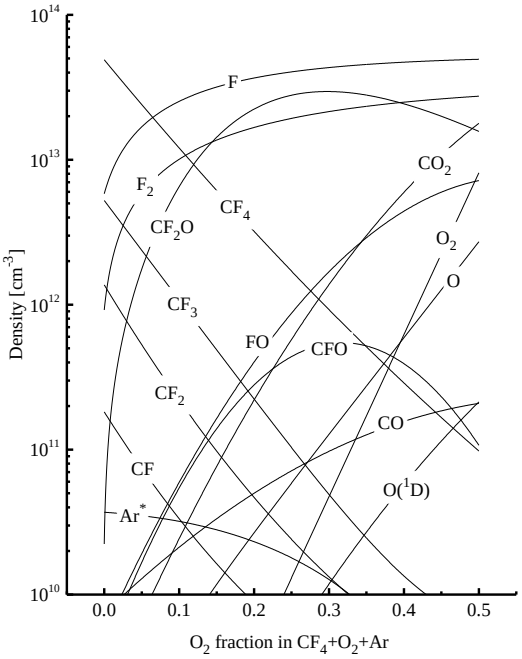

Fig. 2. Model-predicted densities of neutral species as function of O_2 fraction in CF_4 + O_2 + Ar gas mixture

Рис. 2. Расчетные концентрации нейтральных частиц как функции доли O_2 в плазмообразующей смеси CF_4 + O_2 + Ar

The substitution of Ar for O_2 at a constant fraction of CF_4 noticeably reduces the rates of R3–R5, even under the condition of low-oxygenated ($y_{O2} < y_{Ar}$) plasmas (for example, a two-fold decrease at 12% O_2). This is due to the simultaneous decrease in n_e, n_{CF4} ($3.5 \cdot 10^{13}$-$1.9 \cdot 10^{13}$ cm^{-3} for 0-12% O_2), and n_{CF3} ($5.2 \cdot 10^{12}$-$1.9 \cdot 10^{12}$ cm^{-3} for 0-12% O_2). The density of CF_3 radicals decreases because of their decomposition in R10: $CF_3 + O \rightarrow CF_2O + F$, R11: $CF_3 + O(^1D) \rightarrow$ $\rightarrow CF_2O + F$, R12: $CF_3 + CFO \rightarrow CF_4 + CO$ and R13: $CF_3 + CFO \rightarrow CF_2O + CF_2$ with the participation of

O, O(^{1}D), and CFO. The behavior of n_{CF4} follows that of n_{CF3} because the latter represent the main source of CF_4 molecules in the plasma chemical reactions. At the same time, the addition of O_2 introduces new channels for the formation of F atoms involving CFO (R14: CFO + e → CO + F + e) and CF_2O (R15: CF_2O + e → CFO + F + e), while also accelerating R8. The high formation rate for the CFO species is provided by R15 and R16: CO + F → CFO, while CF_2O is effectively formed in R13, R17: 2CFO → CF_2O + CO and R18: CFO + F → CF_2O. The acceleration of R8 is due to the rapidly increasing F_2 density (n_{F2} = $9.2\cdot10^{11}$-$9.0\cdot10^{12}$ cm^{-3} for 0-12% O_2), because of the formation of these species in R19: CF_2O + O(^{1}D) → → F_2 + CO_2 and heterogeneous recombination of F atoms. As a result, the total F atom formation rate increases compared with the CF_4/Ar plasma, which causes an increase in F atom density (n_F = $5.8\cdot10^{12}$-$2.6\cdot10^{13}$ cm^{-3} for 0-12% O_2). The further addition of O_2 in the feed gas and the transition to the high-oxygenated plasmas ($y_{O2} < y_{Ar}$) maintains all the previously mentioned tendencies for reaction rates while also introducing additional mechanisms for the formation of F atoms. Particularly, in the 50% CF_4 + + 50% O_2 gas mixture (y_{O2} = 0.5 and y_{Ar} = 0), the electron impact dissociation rate of the FO species (R20: FO + e → F + O + e) reaches the R14 and R15 levels. The high formation rate and density of FO ($8.2\cdot10^{10}$-$6.3\cdot10^{12}$ cm^{-3} for 12-50% O_2) are provided mainly by R21: F_2 + O(^{1}D) → FO + F and the heterogeneous interaction between F and O atoms. Simultaneously, the total effect of R14, R15 and R20 becomes greater than the sum of R3–R5. Apart from these, the rates of the atom-molecular processes R21, R22: FO + O → F + O_2, R23: FO + O(^{1}D) → F + O_2, R24: FO + FO → 2F + O_2 and R25: CFO + O → CO_2 + F increase together with the increasing O_2 content in the feed gas and, finally, appear to be comparable with R14, R15 and R20. Therefore, the substitution of Ar for O_2 in the CF_4/Ar/O_2 gas mixture under the given conditions provides a continuous increase in the F atom formation rate and thus, the F atom density.

The data discussed above allow one to define clearly the differences between the three-component CF_4/Ar/O_2 (with constant y_{CF4}) and "classical" two-component CF_4/O_2 gas systems. In the CF_4/O_2 gas mixture, the addition of O_2 at constant p results in a proportional decrease of CF_4 fraction in a feed gas. This fact results in a faster decrease in the densities of both CF_4 and CF_3 (compared with those mentioned by Fig. 2) as well as in slower increase in F_2, CFO, CF_2O, and FO densities. In fact, the formation rates for these species appear to be strongly limited by the lack of fluorine coming with the feed gas. As a result, the densities of F_2, CFO, CF_2O, and FO exhibit maximums in the range of 30-50 % O_2 that is directly reflected on the behavior of the F atom density through the non-monotonic rates of R8, R14, R15, R20 and R22–R24.

Another important issue for the dry etching process analysis is the efficiency of the ion bombardment which determines the contribution of the physical etching pathway to the overall process rate. In the ion-assisted chemical reaction, the role of ion bombardment may include the sputtering of the native surface atoms, the ion-stimulated desorption of low-volatility reaction products, and the destruction of the fluorocarbon film. From Refs. [17, 18], it can be understood that the rate of the physical etching pathway is given by $Y_S\Gamma_+$, where $\Gamma_+ \approx J_+/e$ is the total flux of the positive ions on the etched surface and Y_S is the ion-type-averaged sputtering yield. For the ion bombardment energy, ε_i < 500 eV, one can assume Y_S to be proportional to the energy transferred by the incident ion to the surface atom [17]. Therefore, the physical etching pathway can be characterized by the ion energy flux $\varepsilon_i\Gamma_+$, where $\varepsilon_i \approx e|-U_f-U_{dc}|$. From Fig. 1(c), it can be seen that the parameter $-U_{dc}$ increases toward O_2-rich plasmas in the range of 137-153 V. The weakly increasing ε_i compensates for the fall of Γ_+, so that the parameter $\varepsilon_i\Gamma_+$ keeps a near-to-constant value for 0-50% O_2. Therefore, the substitution of Ar for O_2 in CF_4/O_2/Ar gas mixture has no noticeable influence on the efficiency of the physical etching pathway.

Finally, we would like to pay the attention to some relative parameters which characterize the influence of both chemical and physical effects on the dry etching kinetics in the given gas system. The opposite changes in F and CF_x densities mentioned by Fig. 2 result in the F/CF_x flux ratio of 8-13000 for 0-50% O_2. Additionally, the ion/CF_x and O/CF_x flux ratios also increase toward O_2-rich plasma by more than two orders of magnitude, in the ranges of 0.6-98 and 0-795, respectively. All these mean that the substitution of Ar for O_2 creates a favorable condition for etching, but not for polymerization. Therefore, as the O_2 fraction in a feed gas increases, one can expect the higher etching rates together with lower residues of the FC polymer on the etched surface.

REFERENCES

1. **Rossnagel S.M., Cuomo J.J., Westwood W.D.** Handbook of plasma processing technology. Noyes Publications, Park Ridge. 1990. 338 p.
2. **Rooth J.R.** Industrial Plasma Engineering. Philadelphia: IOP Publishing LTD. 1995. 620 p. DOI: 10.1201/9781420050868.

3. **Roosmalen A.J., Baggerman J.A.G., Brader S.J.H.** Dry etching for VLSI. New-York: Plenum Press. 1991. 490 p. DOI: 10.1007/978-1-4899-2566-4.
4. **Wolf S., Tauber R.N.** Silicon Processing for the VLSI Era. Volume 1. Process Technology. New York: Lattice Press. 2000. 416 p.
5. **Kimura T., Noto M.** Experimental study and global model of inductively coupled CF_4/O_2 discharges. *J. Appl. Phys.* 2006. V. 100. P. 063303. DOI: 10.1063/1.2345461.
6. **Plumb I.C., Ryan K.R.** A model of chemical processes occurring in CF_4/O_2 discharges used for plasma etching. *Plasma Chem. Plasma Proc.* 1986. V. 6. P. 205-230. DOI: 10.1007/BF00575129.
7. **Venkatesan S.P., Trachtenberg I., Edgar T.F.** Modeling of silicon etching CF_4/O_2 and CF_4/H_2 plasmas. *J. Electrochem. Soc.* 1990. V. 137. N 7. P. 2280–2290. DOI: 10.1149/1.2086928.
8. **Schoenborn P., Patrick R., Baltes H.P.** Numerical simulation of a CF_4/O_2 plasma and correlation with spectroscopic and etch rate data. *J. Electrochem. Soc.* 1989. V. 136. N 1. P. 199–205. DOI: 10.1149/1.2096585.
9. **Kim M., Min N.-K., Efremov A., Lee H.W., Park C.-S., Kwon K.-H.** Model-based analysis of the silica glass film etch mechanism in CF_4/O_2 inductively coupled plasma. *J. Mater. Sci.: Mater. Electron.* 2008. V. 19. P. 957-964. DOI: 10.1007/s10854-007-9425-z.
10. **Kwon K.-H., Efremov A., Kim M., Min N.K., Jeong J., Kim K.** Model-Based Analysis of Plasma Parameters and Active Species Kinetics in Cl_2/X (X=Ar, He, N_2) Inductively Coupled Plasmas. *J. Electrochem. Soc.* 2008. V. 155. P. D777-D782.
11. **Kwon K.-H., Efremov A., Kim M., Min N.K., Jeong J., Kim K.** A model-based analysis of plasma parameters and composition in HBr/X (X=Ar, He, N_2) inductively coupled plasmas. *J. Electrochem. Soc.* 2010. V. 157. P. H574-H579. DOI: 10.1149/1.3362943.
12. **Johnson E.O., Malter L.** A floating double probe method for measurements in gas discharges. *Phys. Rev.* 1950. V. 80. P. 58-70. DOI: 10.1103/PhysRev.80.58.
13. **Sugavara M.** Plasma etching: Fundamentals and applications. New York: Oxford University Press. 1998. 469 p.
14. **Lim N., Efremov A., Yeom G.Y., Kwon K.-H.** On the etching characteristics and mechanisms of HfO_2 thin films in CF_4/O_2/Ar and CHF_3/O_2/Ar plasma for nano-devices. *J. Nanosci. Nanotechnol.* 2014. V. 14. N 12. P. 9670-9679. DOI: 10.1166/jnn.2014.10171.
15. **Lee J., Efremov A., Lee J., Yeom G.Y., Kwon K.-H.** Silicon surface modification using C_4F_8+O_2 plasma for nanoimprint lithography. *J. Nanosci. Nanotechnol*. 2015. V. 15. N 11. P. 8749-8755. DOI: 10.1166/jnn.2015.11511.
16. **Bose D., Rauf S., Hash D.B., Govindan T.R., Meyyappan M.** Monte Carlo sensitivity analysis of CF_2 and CF radical densities in a c-C4F8 plasma. *J. Vac. Sci. Technol.* A. 2004. V. 22. P. 2290-2298. DOI: 10.1116/1.1795826.
17. **Jin W., Vitale S.A., Sawin H.H.** Plasma-surface kinetics and simulation of feature profile evolution in Cl_2+HBr etching of polysilicon. *J. Vac. Sci. Technol.* A. 2002. V. 20. P. 2106-2118. DOI: 10.1116/1.1517993.
18. **Gray D.C., Tepermeister I., Sawin H.H.** Phenomenological modeling of ion enhanced surface kinetics in fluorine-based plasma etching. *J. Vac. Sci. Technol.* B. 1993. V. 11. P. 1243-1257. DOI: 10.1116/1.586925.

Поступила в редакцию 31.10.2016
Принята к опубликованию 12.01.2017

Received 31.10.2016
Accepted 12.01.2017